Table 2.2.1 (Continued)

	AUTHOR (DATE)	TOPOGRAPHIC SITE	PROBLEM STUDIED	TYPE OF AIRFLOW	MAXIMUM HEIGHT OF FEATURE (m)	LENGTH SCALE RATIO	delta/H	alpha	Similitude Criteria $Z_o/H \times 10^4$	u'/U_*	u_*/U_*	L_u/H	RI or PG Category
34	Meroney, et.al. (1976) CSU	Idealized hills Shapes: 2D	Topographic effects for WECS	Neutral			10.00	0.14	1.00	0.15	0.03		
				Barostromatic			10.00		1.00				
	(1977)	2D		Neutral			10.00	0.14	1.00	0.15	0.03		
	(1978)	3D											
*35	Kitabayashi (1977) CSU	Idealized hills	Stagnant Flows	Barostromatic			3.00						0.19–2.78
36	Petersen, Cermak & Ayad (1977–78) CSU	Geysers Area, California	Topographic effects Diffusion	Neutral	700	1920	2.50		7.00				
37	Cermak & Mutter (1977–78) CSU	Kahe, Oahu	Topographic effects Diffusion	Neutral	900	6500							
*38	Govind, et.al. (1977–78)	Kingston, TN	Topographic effects Diffusion	Neutral	150	800							
39	Ukeguchi, Okamato, Maeda & Chiba (1977)	Various terrain Japan	Nuclear power station Diffusion	Neutral		1000–2000							
*40	Meroney et.al. (1978) CSU, U. of Canterbury	Rakaia Gorge New Zealand	Topographic effects for WECS	Neutral	200	5000	2.50	0.15	1.00	0.13	0.03	0.75	
*41	Petersen and Cermak (1978) CSU	Geysers Area, California	Topographic effects Diffusion	Neutral	700	1920	2.15		0.15				0.06
*42	Graham, et al. (1978) CSU	Terrain near Kingston, Tenn	Topographic effects Diffusion	Neutral	100	960	6.34			0.2–0.3	0.1–0.2		
43	Hunt, Snyder & Long (1978)	Generic hill	Dividing streamline	Stable									6–25
44	Petersen and Cermak (1979) CSU	ASARCO Smelter Hayden, Arizona	Topographic effects Diffusion	Neutral	550	1920	2.09	0.07–0.60	0.06	0.2–0.3	0.03–0.21		
*45	Chien, Meroney, & Sandborn (1979) CSU	Kahuku Point Oahu, Hawaii	Topographic effects for WECS	Neutral	293	3840	4.78	0.13–0.15	3.75	0.17–0.18	0.02	0.57	
46	Petersen, Cermak & Hisato (1980) CSU	ASARCO Smelter Hayden, Arizona	Topographic effects Diffusion	Stable	550	3072	2.23	0.18–0.42	7–255		0.09		0.53
*47	Petersen and Cermak (1980) CSU	Alkali Creek	Topographic effects	Stable/Neutral	1100	1920		0.07–0.23	0.002–14		0.03–0.06		3–14.2
		Coal Creek Crested Butte, CO	Diffusion	Stable/Neutral	1000	2560		0.18–0.30	6.90		0.05–0.08		0.07–2.2
*48	Briatore, Elisei & Longhetto (1980)	La Spezia coast Italy	Topographic effects Diffusion	Stable/Neutral	673	1800	5.20						
*49	Alessio, Briatore, Elisei & Longhetto (1981)	Grosseto, Italy	Dense plumes Valley flows	Stable	120	250, 3000, 4000							
50	Arya, et al. (1979–81)	Generic hills Two dimensional	Topographic effects Diffusion	Neutral									
51	Khurshudyan, Snyder & Nekrasov (1981)	Generic hills Two dimensional	Topographic effects Diffusion										

Table 2.2.1 (Continued)

	AUTHOR (DATE)	TOPOGRAPHIC SITE	PROBLEM STUDIED	TYPE OF AIRFLOW	MAXIMUM HEIGHT OF FEATURE (m)	LENGTH SCALE RATIO	delta/H	alpha	Similitude Criteria $Z_o/H \times 10^4$	u'/U_*	u_*/U_e	L_w/H	RI or PG Category
52	Snyder, et al. (1980–85)	Triangular ridges Sinusoidal ridges Fences	Topographic effects Diffusion Dividing streamline	Stable/Neutral									
*		Cinder Cone Butte Witch of Agnesi			100	690							
53	Lee, Barr, Snyder & Lawson (1981)	Generic long valley	Valley channeling	Neutral			10.00						
54	Pearse, Lindley & Stevenson (1981)	Generic hills Two dimensional	Topographic effects for WECS	Neutral									
54	Pearse (1982)	Generic conical hills	Topographic effects for WECS	Neutral	15	300	18.00	0.17		0.25		120.00	
*55	Neal (1983)	Gebbies Pass in Banks Peninsula, NZ	Topographic effects for WECS	Neutral	300	4000, 8000	2.13			0.10			
*56	Falvey (1983)	American river basin California	Topographic effects Diffusion	Stable	2600	250000 horiz. 125000 vertic.							
57	Ohba & Nakamura (1983)	Generic hills Two dimensional	Topographic effects Diffusion	Stable/Neutral									0.0, 0.7, 1.8
58	Castro, Snyder & Marsh (1983)	Generic hills Three dimensional	Topographic effects Diffusion	Stable									0.39–25
*59	Ohba & Nakamura (1983)	Coastline Japan	Topographic effects Diffusion	Stable/Neutral	175	2000	2.86						0.1, 0.8, 2.1, 2.9
*60	Teunissen, et al. (1982–86)	Askervein hill Outer Hebrides, Scotland	Topographic effects for WECS	Neutral	116	800 1200 2500	2.76 2.33 1.98	0.19 0.14 0.14	3.10 0.51 0.60	0.16 0.12 0.11	0.05 0.04 0.04		
61	Tampieri & Hunt (1985)	Generic valleys Two dimensional	Topographic effects Diffusion	Stable									0.31–16
62	Arya & Gadiyaram (1986)	Generic hills Three dimensional	Topographic effects Diffusion	Neutral			4.00	0.13	3.00	0.12			
63	Lohmeyer & Plate (1986)	Generic hills Three dimensional	Topographic effects Windblown dusts Diffusion	Neutral				0.12		0.15			
64	Neff & Meroney (1987) CSU	Savannah River Lab. South Carolina	Topographic effects Diffusion	Neutral Stable Neutral Unstable		400 1000 1000 1000		 0.23 0.00		0.24 0.07 0.24 0.23	 0.003 0.024 0.040		D B D F
*65	Salmon, Teunissen, Mickle & Taylor (1988)	Kettle Hill Alberta, Canada	Topographic effects	Neutral	100	1000							

Table 2.2.1 (Concluded)

	AUTHOR (DATE)	TOPOGRAPHIC SITE	PROBLEM STUDIED	TYPE OF AIRFLOW	MAXIMUM HEIGHT OF FEATURE (m)	LENGTH SCALE RATIO	delta/H	alpha	Similitude Criteria $Z_o/H \times 10^4$	u'/U_*	u_*/U_*	L_w/H	RI or PG Category
66	Briggs, Thompson & Snyder (1989)	Valley Two dimensional	Topographic effects Diffusion	Neutral but stable valley air									
67	Gong & Ibbetson (1989)	Generic hills Two dimensional Three dimensional	Topographic effects on WECS	Neutral									
68	Finnigan, Raupach, Bradley & Aldis (1990)	Rough generic hill Two dimensional	Topographic effects	Neutral									
*69	Meroney & Neff (1989–90) CSU	Jusupa Mountains California	Topographic effects Diffusion	Neutral Stable	420	1000 2500	4.50 5.40	0.17 0.28	7.62 7.62	0.25 0.03–0.05	0.0021		D E–F

* Field observations available

III. WIND FLOW OVER VEGETATIVE CANOPIES

As early as 1893, a German scientist, Metzger, investigated the effects of wind action on trees. Subsequently, a variety of studies have been made of the behavior of winds well inside and directly above a forest canopy (Bayton, 1963; Cooper, 1965; Denmead, 1964; Dolman, 1986; Fons, 1940; Grant, 1984; Huston, 1964; Poppendiek, 1949; Sadeh et al., 1982; Sauer et al., 1951; Tiren, 1927; Tourin and Shen, 1966; etc.). Some measurements are available for the variation of the wind at the edge of a forest (Iizuka, 1952; Leahey and Hansen, 1987; Reifsnyder, 1955). Much of this data is accumulated in periodically issued reviews and books (Geiger, 1956; Monteith, 1976; Raupauch and Thom, 1981; Forests, Weather and Climate, 1989).

Laboratory simulation of canopy flow in the wind tunnel has been used by the forest meteorologist in his efforts to understand the complex nature of flow generated by the tree--a permeable, random shaped, elastic object. Tiren, 1927, attempted to estimate crown drag from conifer branch-drag measurements made in a wind tunnel as part of his study of stem forms. Wind-breaks have been studied by models to determine soil erosion and blow-down characteristics (Hirata, 1953; Iizuka, 1956; Malina, 1941; Woodruff and Zingg, 1952). Others performed studies to characterize the transport of scalar products into, within and above vegetation (Plate and Quarishi, 1965, Kawatani and Meroney, 1968; Meroney, Kesic and Yamada, 1968). These studies were conducted to deduce the qualitative behavior of tree barriers for specific problems. The investigators apparently made no attempt to scale dynamically the character of a live tree except to compensate intuitively for shape and porosity.

To model completely the complex geometry and structural characteristics of a live tree is obviously not practical; however, measurements made on coniferous and deciduous trees in the wind tunnel and the field suggest that equivalence of drag and wake characteristics between model and prototype trees should be sufficient to study the general flow phenomenon (Lai, 1955; Meroney, 1968; Rayner, 1962; Sauer et al., 1951; Walshe and Fraser, 1963). Subsequently, a number of studies have been completed with greater attention to the flow characteristics of individual canopy elements (Hsi and Nath, 1968; Finnigan and Mulhearn, 1978; Kawatani and Meroney, 1970; Meroney, 1968, 1969; Raupach et al., 1980; Kawatani, 1971).

These field and laboratory measurements have provided a rough picture of a highly complex and turbulent flow field within the forest canopy. Measurements made behind small to medium specimens of spruce, juniper and pine trees reveal that linear wake growth exists behind all trees, that the wake shadows of individual branches disappear within 1-2 tree crown diameters downstream and that the velocity defect becomes Gaussian within 3-4 crown diameters. Drag measurements made on live trees indicate the drag coefficient, $C_d = F_{drag}/(\frac{1}{2}\rho U^2_{ref} A)$, may vary with wind speed from 1.0 - 0.3 **(Figure 3.0.1)**. These measurements indicate that the flow is inertially dominated (i.e., Reynolds number independent), but that self-streamlining of the tree at high velocities can reduce the effective cross-sectional area for the more flexible species. Measurements made within and above real and model trees reveal quite different flow characteristics for the under-canopy and above-canopy forest regions.

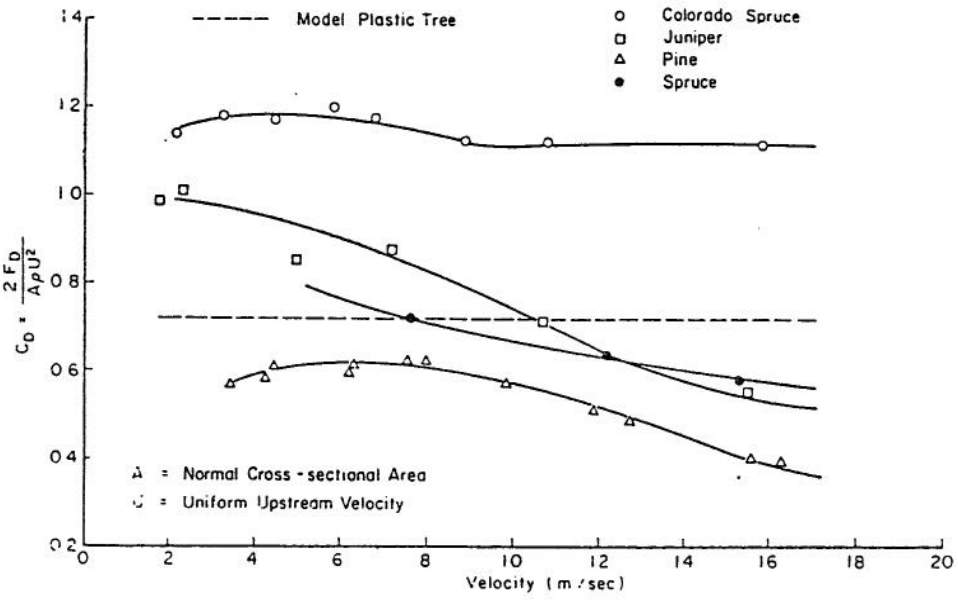

Figure 3.0.1 Drag coefficients of live and model trees: Dashed line (after Hsi and Nath, 1968); solid circles (after Rayner, 1962) (Meroney, 1968)

3.1 Flow Within and Downwind of an Individual Tree

Even a single tree can significantly reduce wind speeds and increase turbulence downwind of its stem and crown. Gross (1987) used a three-dimensional nonhydrostatic numerical model to investigate the air flow and turbulence around a single tree. For turbulence closure he used the Prandtl-Kolmogorov exchange coefficient and the Blackadar mixing length relation. The presence of the tree is simulated by an additional drag coefficient associated with tree foliage density or leaf area density. Time integrated solutions are obtained by the Adams-Bashforth scheme, centered differences are specified in space, and a fast Poisson solution solver is used to determine the pressure field.

Calculations were performed for both "cone" and "ball" shaped crown tree regions, with and without elevating trunks, and for neutral and stable air stratification. A tree porosity of 0.934 was assumed based on field measurements, calculations produced the anticipated wake deficits, turbulence excess, and a drag coefficient of 1.0 which are similar to individual tree values measured by Meroney (1968). All simulations show a reduction of wind speed inside the tree foliage, an accelerated flow over and around the tree and a wake region in the lee. The geometry of the crown seems to be the dominant factor. In a stable stratified atmosphere, the flow around the canopy is enhanced, while vertical motion is suppressed, and the strength and length of the reverse flow region behind the tree increases. These results agree well with available field and wind-tunnel experience.

Schematic tree shapes studied are shown in **Figure 3.1.1.** Crown heights considered were 16 m, crown diameters were 13 m, porosity was 0.93, trunk height varied from 0 to 6 m, and approach flow surface roughness was z_o = 0.7 cm. **Figure 3.1.2** displays centerline wake behavior behind a conifer shaped tree with no stem. **Figure 3.1.3** displays excess shear turbulence in the tree wake. **Figure 3.1.4** describes the streamlines of the horizontal airflow 1 m above the ground. The streamline pattern clearly shows the divergence around the tree and the recirculation region behind the tree. **Figure 3.1.5** compares mean velocities in the wake of ball and cone shaped trees elevated on 3 m trunk height.

Persistent strong winds can result in the deformation and growth distortion of individual trees. Hewson et al. (1979) describe methods which permit one to characterize persistent wind directions and speed. **Figure 3.1.6** provides sketches of tree deformation, the associated Griggs-Putnam index number, and the persistent wind velocity that is likely to produce such deformation.

The superposition of individual tree wakes result in the under-forest and above-forest velocity features found in extensive areas of forests or woods. The initial growth of wake deficits and the subsequent decay at greater downwind distances are characteristics of both individual tree and forest measurements.

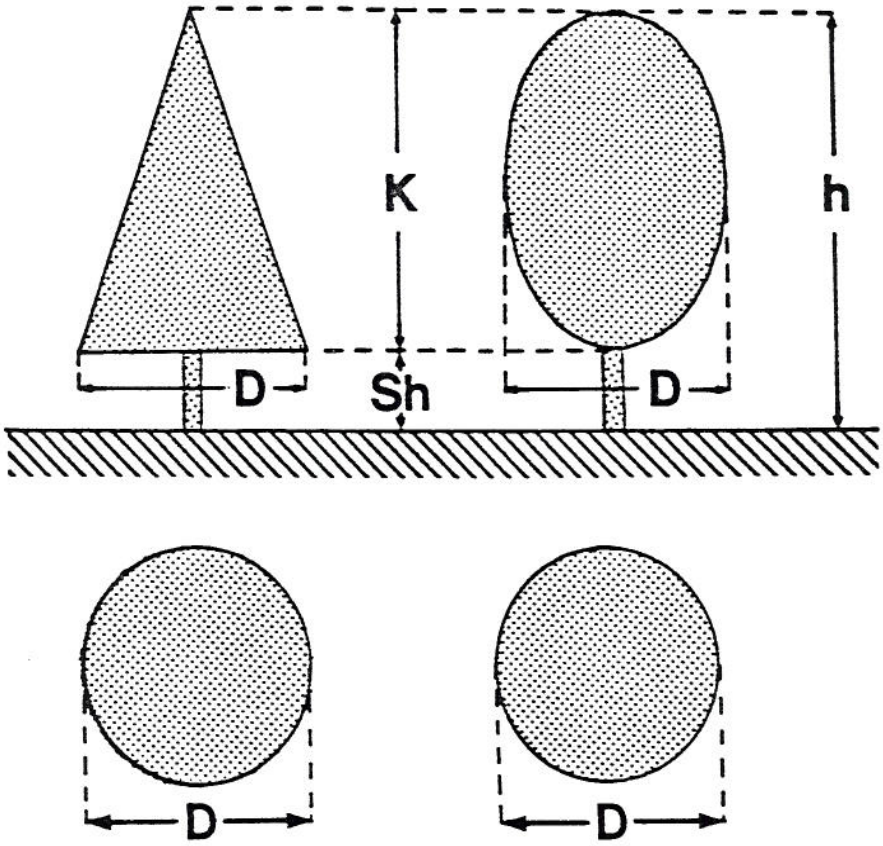

Figure 3.1.1 Geometry of idealized trees for numerical calculations. (Gross, 1987)

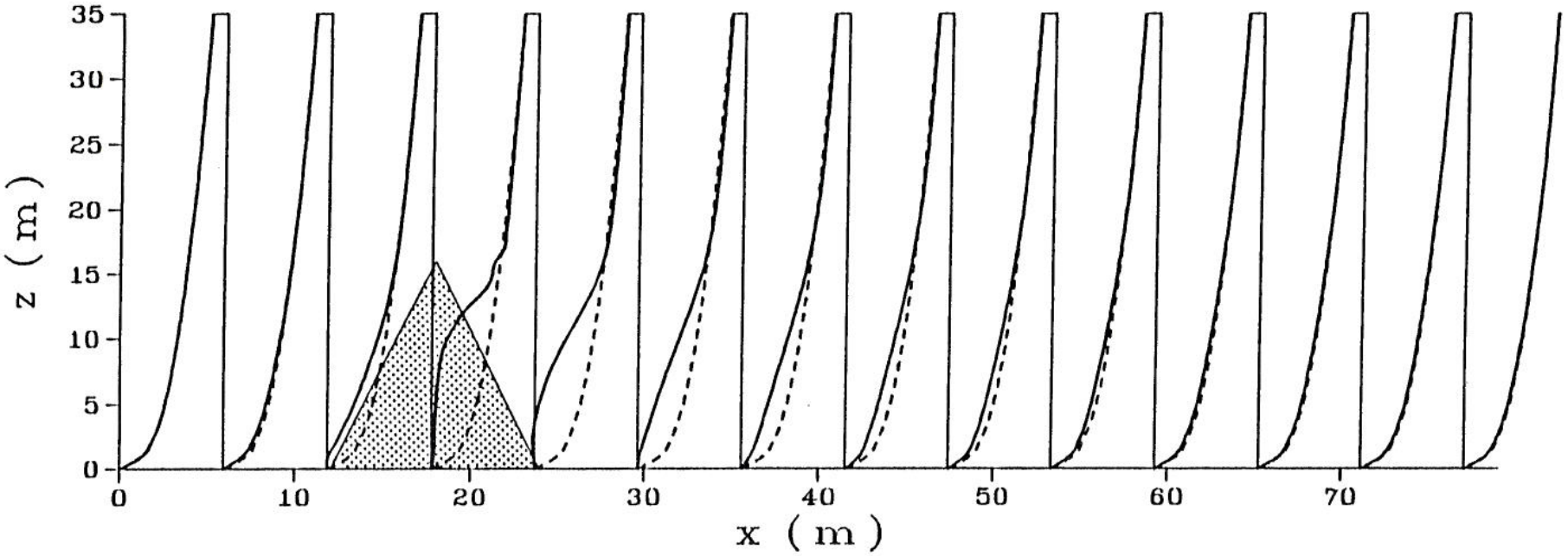

Figure 3.1.2 Vertical profiles of u at different point along the symmetry axis. The dotted line shows the undisturbed profile of the inflow boundary. (Gross, 1987)

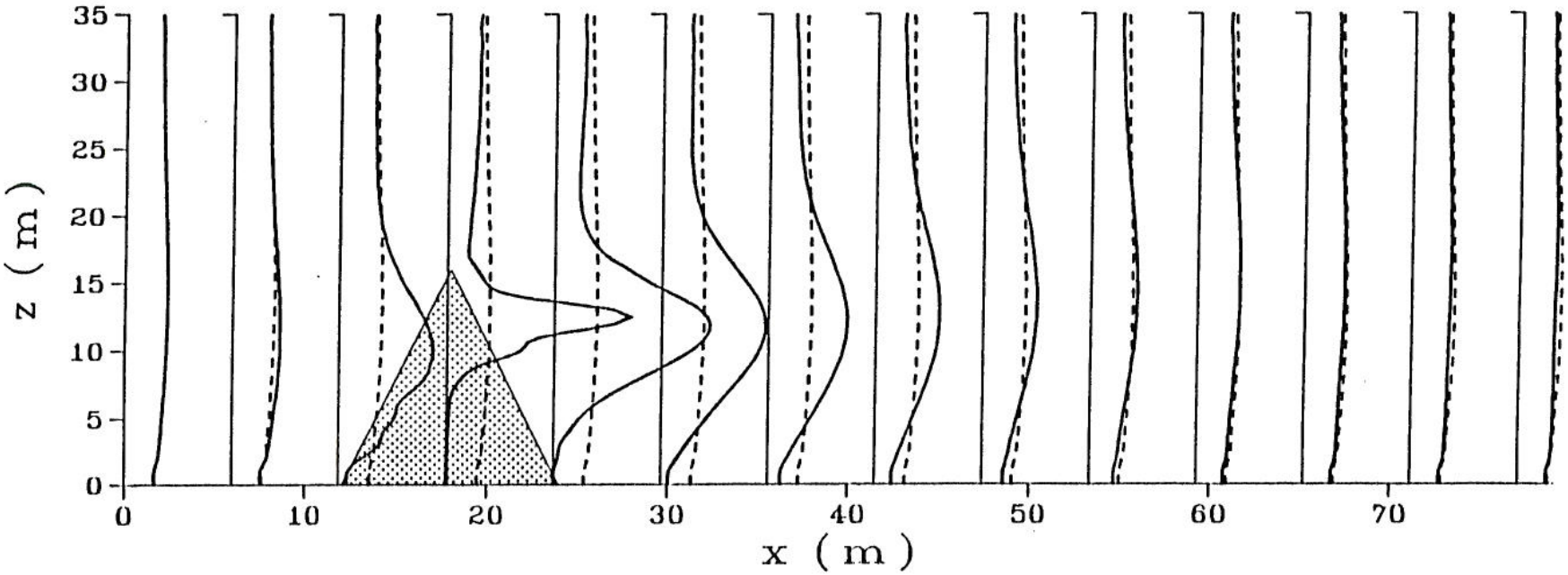

Figure 3.1.3 Vertical profiles of shear stress, σ, at different points along the symmetry axis. The dotted line shows the reference (inflow) value. (Gross, 1987)

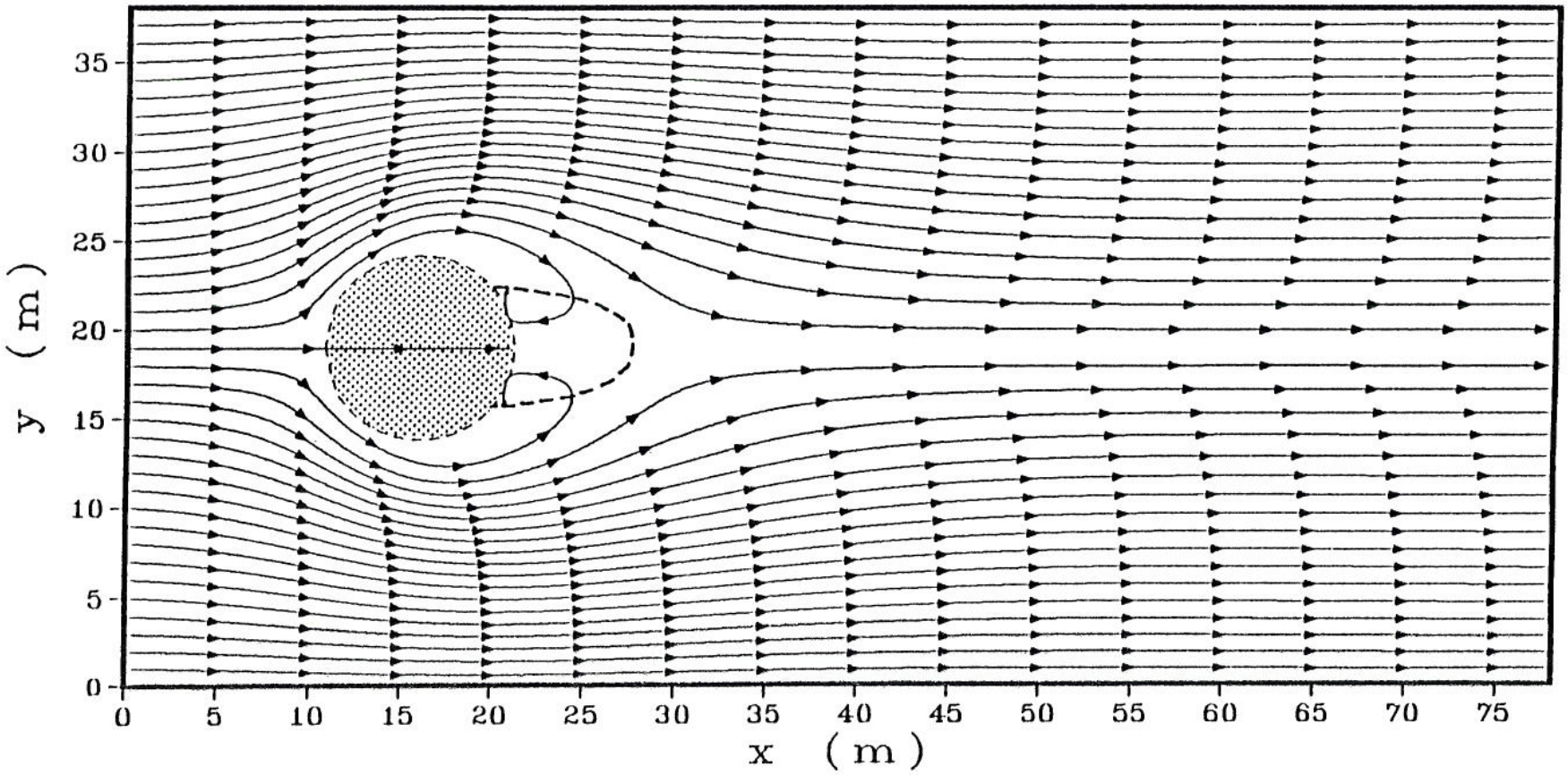

Figure 3.1.4 Streamlines of the horizontal airflow for 1 m above the ground. The contour of the tree is dotted, the dashed line indicates cases where $u < 0$. (Gross, 1987)

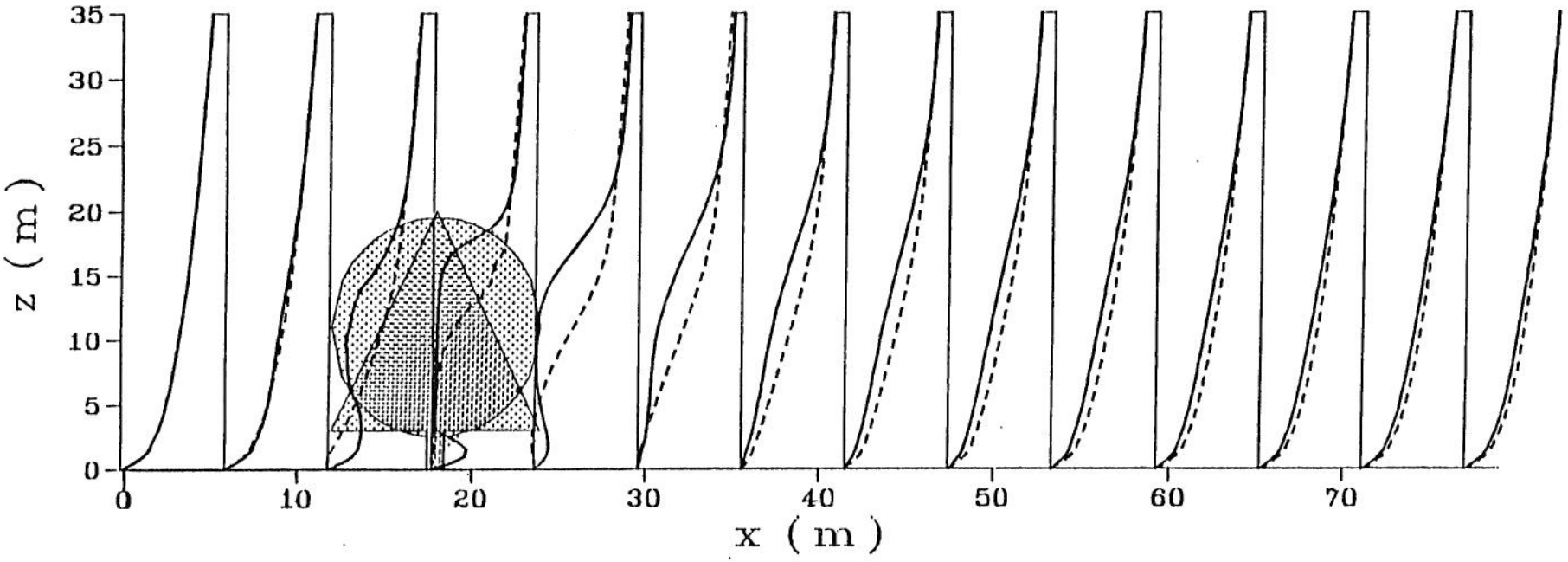

Figure 3.1.5 Vertical profiles of u at different points along the symmetry axis (———— ball-tree, - - - cone-tree) (Gross, 1987)

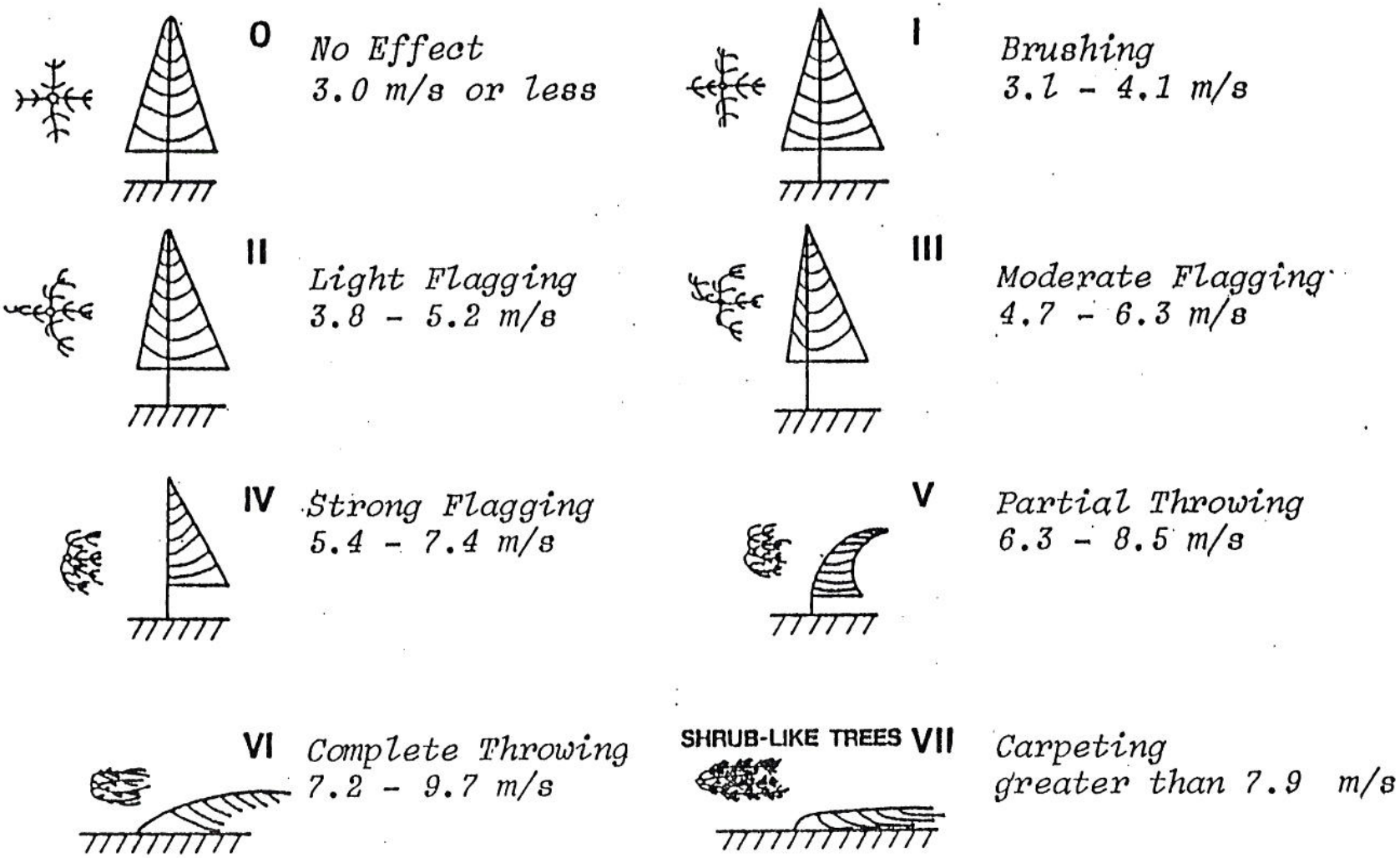

Figure 3.1.6 Wind deformation and the wind velocity that may produce that deformation. (Hewson *et al.*, 1979)

3.2 Under-canopy Forest Flow Field

The presence of tree trunks, branches, stems, and leaves (or needles) in a forest produces a barrier to air flow caused by form drag and skin friction which reduces the under-forest flow velocities substantially compared with wind speeds which occur above the canopy. Surface layer streamlines are displaced vertically, flow beneath the canopy is driven by shear from the flow above the canopy, and maximum winds occur at the top of the average height of the vegetation. Turbulence levels beneath the canopy may be similar to those found at ground level over small roughness surfaces (5-15%), but are significantly less than those which can occur in the strong shear which occurs above the canopy roof (20-40%). **Figures 3.2.1, 3.2.2a and 3.2.2b** display typical mean velocity and turbulence profiles found within and above forest canopies.

Different profiles have been proposed using first order closure models which specify a simple eddy diffusivity, K, and a drag coefficient, C_d, to describe that portion of the mean wind profile which exists beneath the forest ceiling for constant foliage distribution:

$$u/u_h = [(\sinh \beta\xi)/\sinh \beta]^{1/2} \quad \text{(Cowan, 1968),} \quad [3.2.1]$$

$$u/u_h = \exp[-\beta(1 - \xi)/2] \quad \text{(Inoue, 1963; Cionco, 1965), and} \quad [3.2.2]$$

$$u/u_h = [\cosh \beta\xi)/\cosh \beta]^{1/2} \quad \text{(Massman, 1987),} \quad [3.2.3]$$

where $\xi = z/h$, u_h is the mean horizontal wind speed at the top of the canopy, h; and β is a maximum value of the foliage area density and the extinction coefficient given by:

$$\beta = [2C_d \, LAI/(\sigma\mu)]^{1/2}, \quad [3.2.4]$$

which is a combination of the drag coefficient, C_d , the leaf-area-index, LAI, a measure of foliage distribution, σ, and a normalized eddy diffusivity, $\mu = K/hu = K_h /hu_h$. Only the expression proposed by Massman is consistent with the frequently observed zero wind gradient within the lower region of the canopy. Other authors have produced velocity profiles for non-constant foliage distributions and using higher order turbulence closure (Albini, 1981). **Figure 3.2.3** compares the three equations shown above for a $C_dLAI = 0.6$ and constant foliage distributions which result in β values of 4 and 6. For a constant foliage distribution the extinction coefficient β varies from 0 to 10.0 as the function C_dLAI varies from 0.0 to 1.0. Each of the under canopy velocity profiles may be associated with a companion shear stress distribution which looks similar to the velocity distribution. Typical under-canopy measurements made in a Ponderosa pine forest are shown in **Figure 3.2.4** .

Once a velocity distribution model is specified it is possible to solve by iteration for shear stand drag coefficient, $C_f = 2(u_*/u_h)^2$, displacement height, d, and surface roughness, z_o, parameters useful to characterize above canopy flow dynamics as functions of C_dLAI and foliage

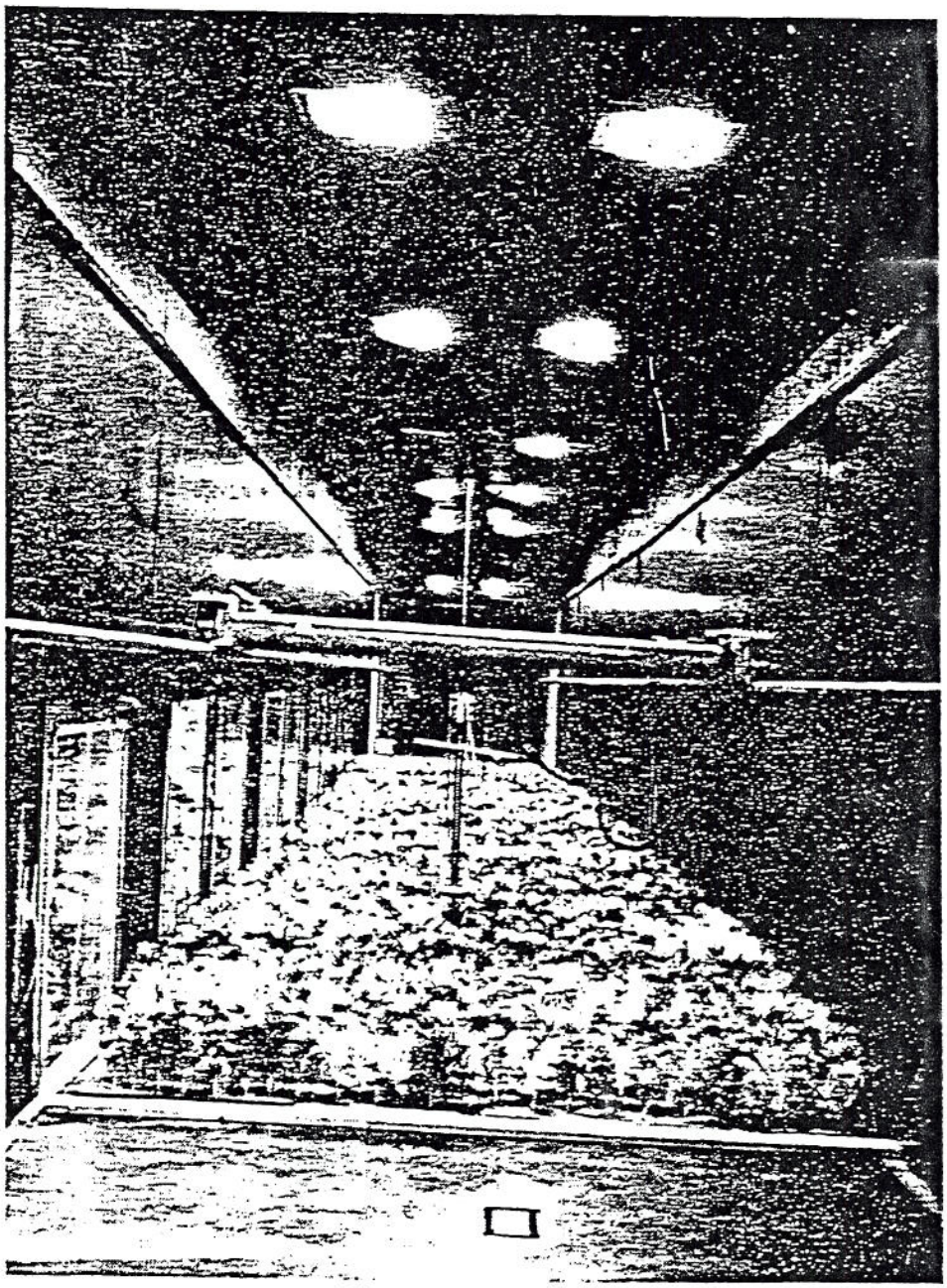

Figure 3.2.1 Meteorological wind tunnel at Colorado State University and artificial tree canopy. (Meroney, 1968)

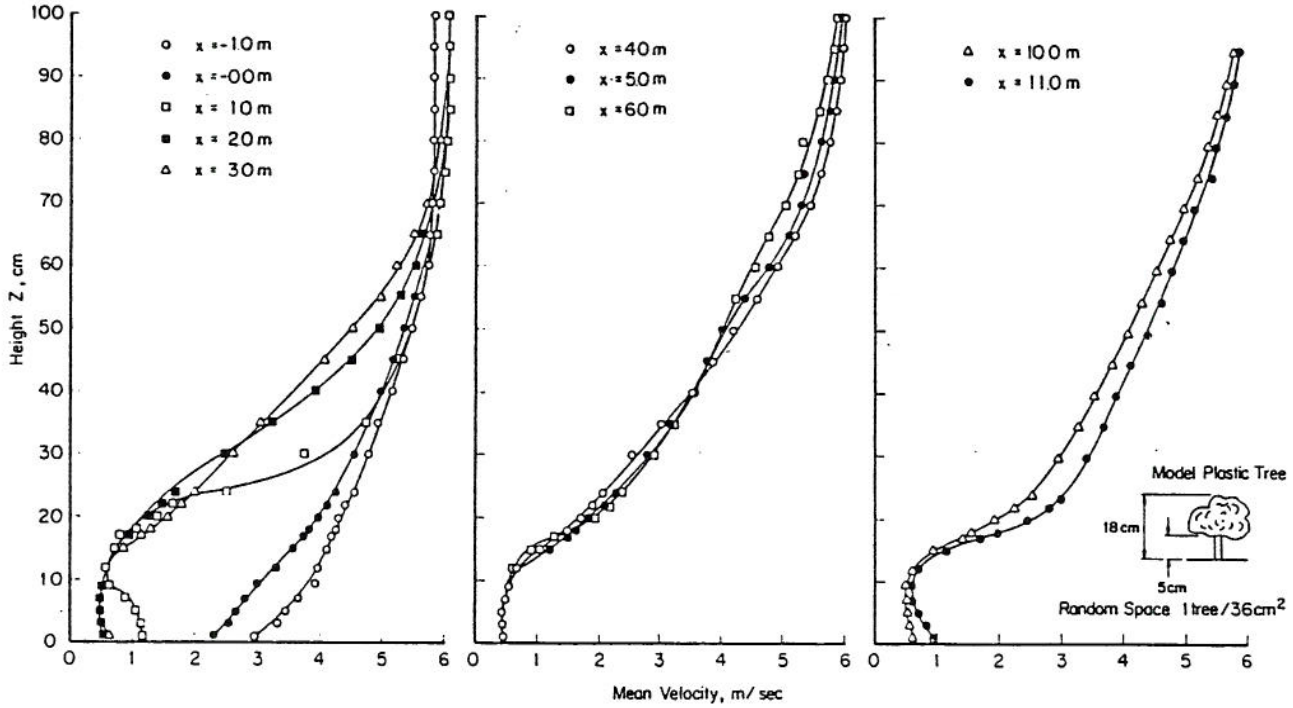

Figure 3.2.2 Velocity profiles in and above model forest canopy (Meroney, 1968)

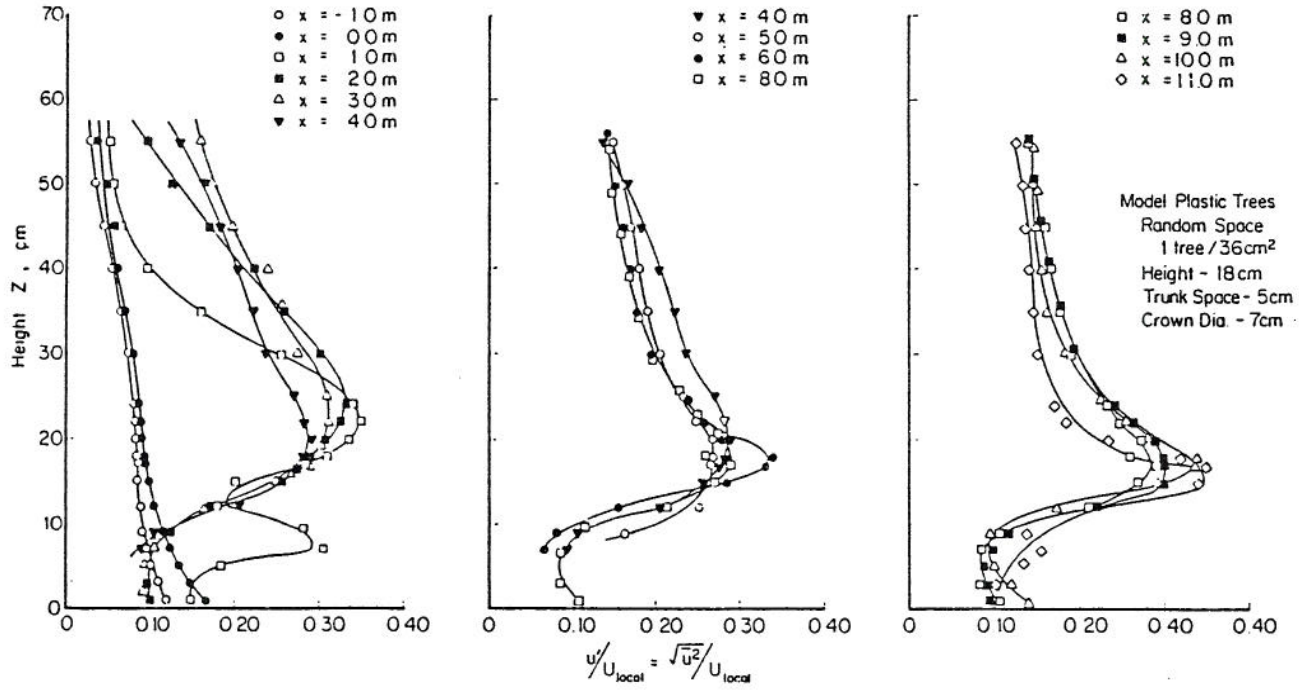

Figure 3.2.2 Longitudinal turbulent intensity for model forest canopy. (Meroney, 1968)

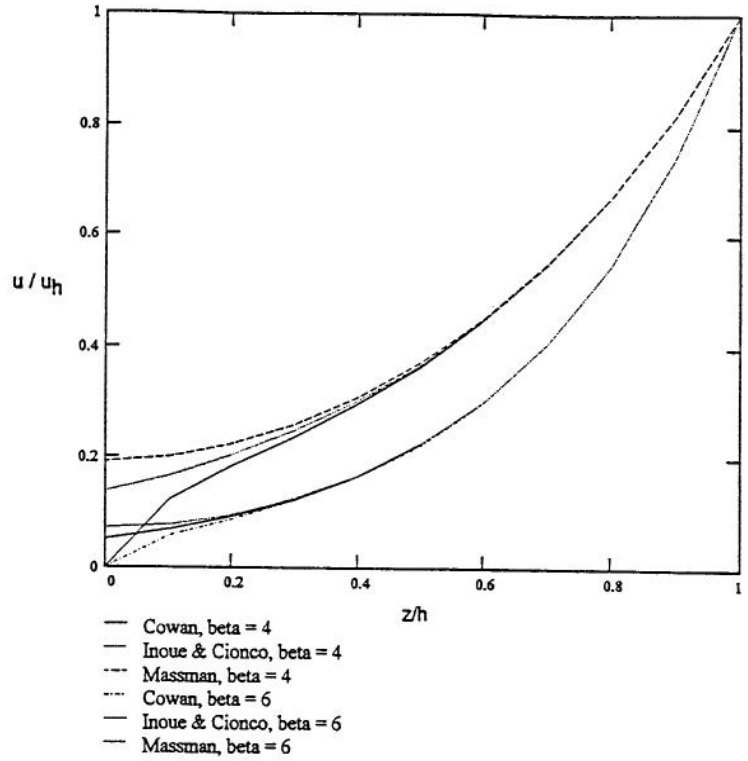

Figure 3.2.3 Under-forest canopy mean velocity profiles for expressions developed by Cowan, 1968; Inoue, 1953, and Cionco, 1965; and Massman, 1987.

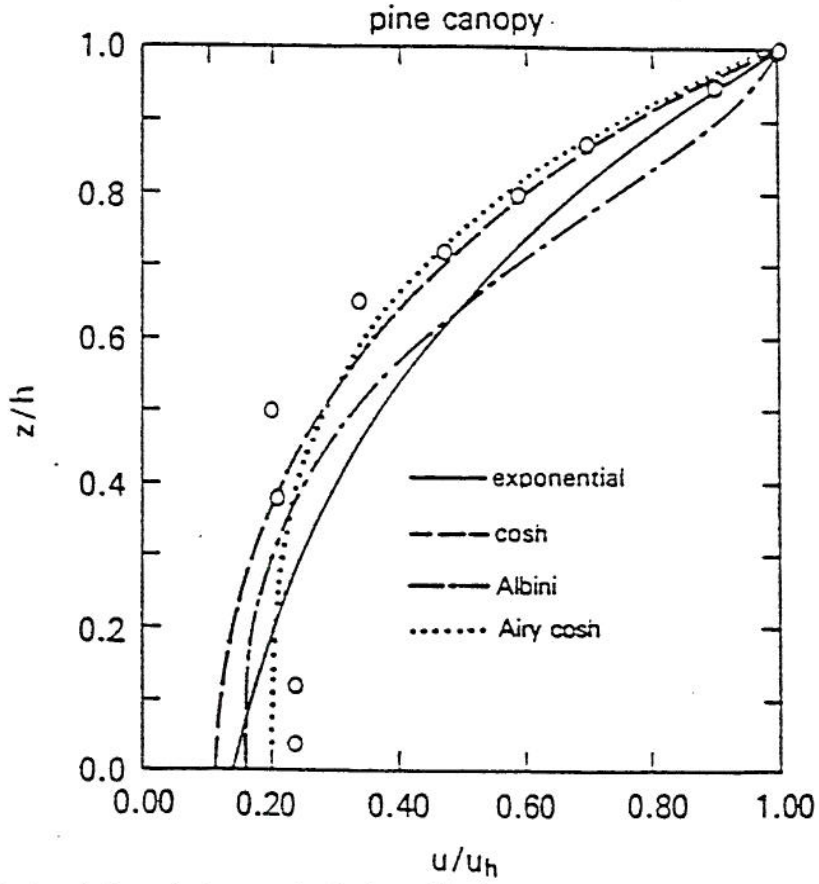

Figure 3.2.4 Optimal fits of observed wind profile for a Ponderosa pine canopy. Observations are denoted by circles from Raupach and Thom (1981).(Massman, 1987)

structure. Massman (1987) concludes that C_dLAI values from 0.25 to 0.50 characterize most full foliage canopies. Over this range almost any under-canopy model gives results very close to the following expressions:

$$0.10 < z_o / h < 0.13, \qquad [3.2.5a]$$

$$0.67 < d/h < 0.75, \text{ and} \qquad [3.2.5b]$$

$$0.17 < C_f < 0.20. \qquad [3.2.5c]$$

3.3 Above-canopy Forest Flow Field

The atmospheric boundary layer (ABL) is that portion of the atmosphere where surface drag due to the motion of the air relative to the ground modifies synoptic-scale motions caused by horizontal pressure gradients, Coriolis forces, and buoyancy. The depth of the ABL is highly variable (50 to 2000 m), but it generally increases with proximity to the equator, with wind speed, and as the earth surface roughens, but it decreases at night, and is strongly modified by thermal winds, inversions, and stratification. Counihan (1975) reviewed all adiabatic ABL data taken between 1880 to 1972. For high wind speeds ($U_{10} > 5$-7 ms^{-1}) Counihan recommended 600 m as a reasonable average boundary layer depth for both rural and urban cases independent of wind speed and roughness.

The lowest 10% of the atmospheric boundary layer is called the surface layer. It is characterized by the sharpest variations of wind speed, temperature, humidity, and turbulence characteristics with height. Counihan (1975) concluded the surface (or constant flux) layer would be about 100 m deep during adiabatic conditions. In diabetic (stratified) situations the surface layer depth is about equal to the absolute value of the Monin Obukhov length, $L_{mo} = -Tu_*^3 / (\kappa g\, w't')$. For a summary of surface layer behavior for both neutral and stratified flows combined with both smooth and rough surfaces see Meroney (1986) or Panofsky and Dutton (1984).

3.3.1 *Logarithmic velocity profile models*

Within the surface layer the mean wind-speed profile is commonly described by logarithmic expressions. For situations when stratification has only a minor influence a modified logarithmic law has been proposed:

$$u(z) = (u_* / \kappa) \ln_e [(z - d + z_o)/z_o], \qquad [3.3.1]$$

where $u_* = (\tau/\rho)^{1/2}$ is the surface friction velocity, d is the zero-plane displacement, κ is Von Karman's shear layer constant, and z_o is the surface roughness. The displacement thickness, d, is important for tall roughness elements such as agricultural crops, forests, and cities. When the roughness elements are short, such that $z_o < 0.2$ m, one can set $d = 0$. The parameters can

be determined from representative field measurements or models such as were discussed in Section 2.2. Fitting an expression which permits three free parameters to field measurements of wind speed in agricultural canopies is not trivial. It is not uncommon for some least-square fitting routines to produce negative displacement heights--which is, of course, inappropriate.

No exact definition of high roughness has been offered, but roughness of a height exceeding 10% of the surface layer is generally viewed as high roughness. (Alternatively, whenever the logarithmic expression with d set equal to zero fails to fit measured wind distributions, the full expression may be justified.) Generally, the von Karman universal constant κ is assumed equal to 0.4 based on extensive experimental study of fully developed turbulent flow through pipes and its relationship to the Kolmogorov dissipation constant. Some experimentalists treat the constant as another free parameter to improve curve fit to data; hence, values ranging from 0.15 to 0.5 have been recorded. Nonetheless, it is customary to accept the initial value of 0.4 unless there are very persuasive arguments to do otherwise.

Some derivations of the logarithmic expression depend upon the assumption that shear stress is nearly constant with height above the surface. Matching of inner and outer similarity solutions to a boundary layer demonstrates, however, that such an assumption is not really necessary to the existence of a region which depends logarithmically on displacement above a ground plane. Nonetheless, the shear stress may be expected to vary substantially above the canopy roof; hence, it would be best to associate the friction velocity with the average drag produced by the wind on the forest. In order to avoid negative displacement height values it is customary to assume the von Karman constant $\kappa = 0.4$, to prespecify displacement height as some fraction of the forest canopy depth (say $d = 0.67$ h) and to solve for friction velocity and surface roughness height by fitting the modified logarithmic expression to measured data.

The effective values of the parameters may vary locally when the surface roughness is non-homogeneous. A non-homogeneous surface occurs when the ground surface changes from water to land, urban to rural, or cleared to forested. Such changes may make it appear that effective surface roughness, surface friction, and displacement height vary with height within the velocity profile. This aspect of the flow field will be discussed further in another section.

Surface roughness estimates have been estimated by many scientists for flow data obtained over different agricultural crops and forests. There is a wide variance in results even for flow over the same surface. Frequently experimentalist fail to obtain data above the wake region of individual roughness elements ($z > 1.5h$); sometimes the data are taken during non-neutral conditions; and often upwind nonhomogenuities distort the measured profiles. Several sets of tabulated data are available prepared by Sutton (1949), Priestly (1959), Davenport, 1960, Counihan (1975), Simiu and Scanlan (1978) and Snyder (1981). See Table 3.3.1 for a summary of such estimates.

Jaeger (1965) recorded wind speed measurements over a ten year period over stands of Scotch pine located in southern Germany as they grew from 3 to 8 m height. He made estimates of the variation in u_*, z_o, d, β (Deacon parameter), and Richardson number, Ri, from wind and

Table 3.3.1 Table of roughness length data

Surface Type	Sutton (1949) (1953) Geiger (1950)	Priestly (1959)	Davenport (1965)	Counihan (1975)	Simiu & Scanlon (1978) & Snyder (1981)
Open sea	0.002-0.05		0.024-0.34	0.001-2	0.0003[a]-0.5[b]
Ice	0.001			0.001-2	
Smooth mud flat	0.001	0.001		0.001-2	
Sand	0.03-0.1	0.03			0.01-0.1
Snow on grass Snow on prairie	0.02 0.3	0.005 0.1		0.001-2	
Mown grass, 1 cm 3 cm 4.5 cm	0.1-0.2 0.7-2.0	0.2 0.7 1.7-2.4			0.1-1
Flat open country	2.0-3.0		1.75-6.5		
Low grass, steppe	1.0-4.0			0.1-20	1-4
Fallow field	5.0			0.1-20	2-3
High grass	3.0-9.0	3.7-9		0.1-20	4-10
Paletto	3.0-14.0				10-30
Pine forest (h = 15 m, d = 12 m)	20.0			100-150	90-100
Outskirts of towns, suburbs			20-90	100-150	20-40[c]
Centers of towns					35-45[c]
Centers of large cities			125-550		60-80[c]

[a] Wind speed at 10 m above sea surface equals 1.5 m/sec

[b] Wind speed at 10 m above sea surface is greater than 15 m/sec

[c] These values are exceptionally small

temperature data collected from meteorological towers placed within the forest stand. He found that the following correlations described the measurements:

$$d = 0.63\ h, \qquad \text{regression coefficient, } r = 0.73\text{-}0.93; \qquad [3.3.2a]$$

$$z_o = 0.174\ h + 0.227, \qquad \text{regression coefficient, } r = 0.44; \text{ and} \qquad [3.3.2b]$$

$$u_* = (0.027\ h + 0.062)\ U_{9.6m} + b, \qquad \text{regression coefficient, } r = 0.84. \qquad [3.3.2c]$$

The expressions for d and z_o are seen to be similar to those derived from examination of under-canopy flows. However, the correlation for z_o is rather poor, and in a personal communication Massman suggested universal expressions for friction velocity are not reliable.

Figure 3.3.1 display the variation of above-canopy wind speeds for typical forest values of displacement height and roughness where $d = 0.67\ h$, $z_o = 0.125\ h$, and $u_* = u(h) \int (C_f/2) = 0.316u(h)$. Given these dimensions one finds that the modified logarithmic law becomes:

$$u(z) = 0.316(u(h)/\kappa)\ln_e[8z/h - 4.34]. \qquad [3.3.3]$$

Of course, this expression is only approximate, since it assumes independence from drag coefficient, leaf area index, and foliage distribution variations. The expression should not be applied below $z = 1.5\ h$.

Estimates of surface drag, roughness and displacement are also sought for use in meso-scale models where combinations of hilly terrain and vegetation can produce an "effective surface roughness" for flows above moderate heights. As noted by Taylor et al. (1989), "momentum transfer at the earth's surface can be considered as part 'skin friction' and part 'form drag.'" One can associate the surface shear stress as that portion of the drag associated with the roughness elements whose dimensions are of order size10 m or less. These include vegetation, buildings and small topographic features like ditches and embankments. The 'form drag' component of the momentum transfer is associated with terrain averaged over the minimum numerical grid used. In addition in stratified flow one may have 'wave drag' associated with waves propagating away from larger features (mountains, hills, and valleys). Taylor et al. used mixing length , turbulent kinetic energy closure, and Reynolds stress closure models to predict velocity profiles over sinusoidal roughness covered with different size surface roughness.. Logarithmic models were then fit to these profiles. A regression on the various calculations agrees with the following semi-empirical expression:

$$\ln[z_o^{eff}/z_o] = 3.5(ak)^2\ln[\lambda/z_o], \qquad [3.3.4]$$

where the surface terrain profile fits $z_s = a\cos(kx)$ and $k = 2\pi/\lambda$. This equation works well for $ak < 0.2$ and not bad at $ak = 0.3$ at which separation probably occurs over the hill crests. Thus, for cases with $\lambda = 500$ m and surface roughnesses, z_o , of 0.01, 0.1 and 1 m, the postulated maximum values of z_o^{eff} will be 2.37, 7.4, and 23.1 m, respectively.

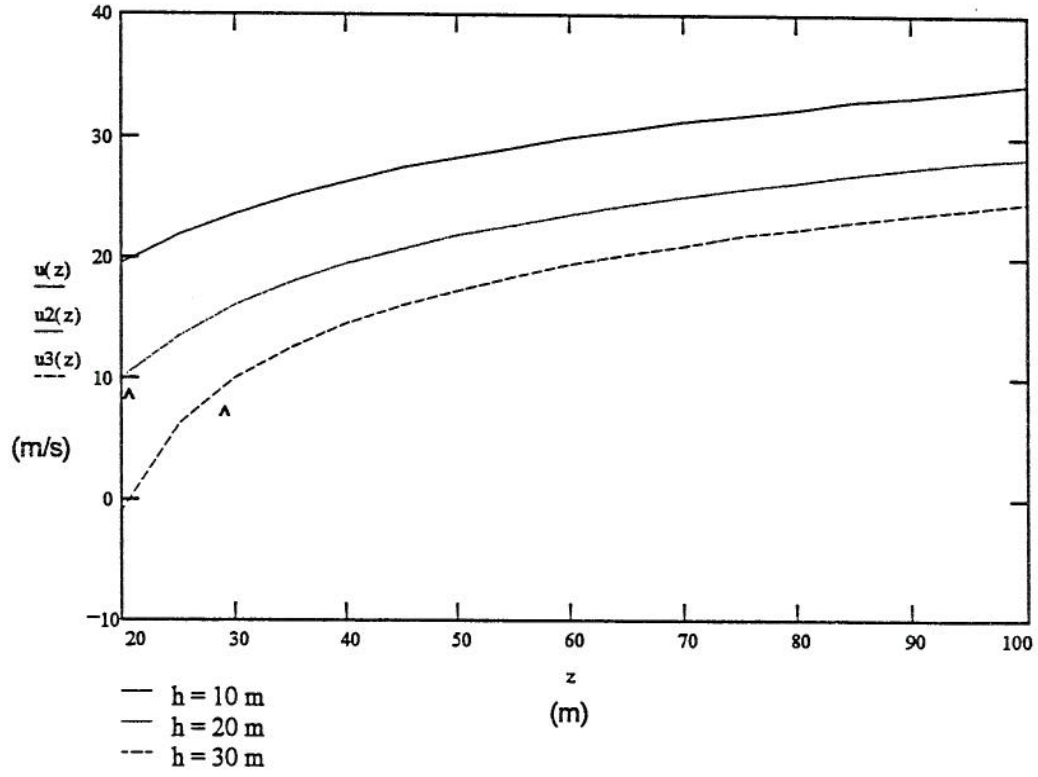

Figure 3.3.1 Above canopy wind profiles for various average forest canopy heights when d = 0.63 h, z_o = 0.125 h, and u_* = 0.316 u(h).

Grant and Mason (1990) reported the results of tether balloon measurements of flow over forest covered complex terrain in southern Wales, U.K. They wished to characterize the effective roughness over areas of the order of 100 km^2. Grant and Mason also generated wind data numerically with a two-dimensional, nonhydrostatic model using a second-order turbulence closure scheme over a hypothetical sinusoidal terrain with horizontal wave length of 2000 m and a peak-to-trough height of H = 300 m. The model was used to verify field measurements and expressions relating terrain undulation and local vegetative roughness.

Grant and Mason also propose that total drag is composed of two parts, a form drag term which represents the drag due to the main orographic elements and a shear stress term due to small scale features such as vegetation. They combined a shear stress estimate at the half-height of the terrain undulation, H/2, with the widely used formulae suggested by Lettau in 1969, $z_o/H = CA/S$, where A is the silhouette area of the roughness elements located in a horizontal area, S. The final expression is:

$$\ln^2 [H/(2z_o^{eff})] = \kappa^2 /\{0.5\ DA/S + \kappa^2/\ln^2[H/(2z_{o1})]\}, \qquad [3.3.5]$$

where D is a drag coefficient. For sinusoidal terrain, D = 0.3. The silhouette area should be averaged over about 12 km. As noted in **Figure 3.3.2** the effective roughness length, z_o^{eff}/H, is found to increase from 0.003 to 0.05 as A/S increases from 0 to 0.2.

3.3.2 *Power-law velocity profile models*

In an alternative empirical approach to describe the wind variation with height the velocity variation is described by a simple power law of elevation. It is widely used in describing the wind shear in the atmospheric surface and internal boundary layers in view of its simple format and engineering expediency. The general form of the expression used is:

$$u(z)/u_{ref} = (z/z_{ref})^{\alpha}, \qquad [3.3.6]$$

where u_{ref} is the reference wind at a reference height z_{ref}, and α is the power law index (exponent). The effect of turbulence induced by the surface roughness upon the wind shear is accounted for by the magnitude of the power law index, whose magnitude is normally smaller than unity but larger than zero. Often the power law index is determined empirically by fitting the expression above to measured data; however, it is also possible to match the magnitude of predicted velocity and shear at a specified height and relate the power law index, α, to logarithmic parameters (z_o, d, and L_{mo}). For neutral flow the expression is simply:

$$\alpha = z_m /[(z_m - d + z_o)(\ln_e [(z_m - d + z_o)/z_o)/z_o], \qquad [3.3.7]$$

where z_m is the matching or mid-height over which both profiles are presumed valid.

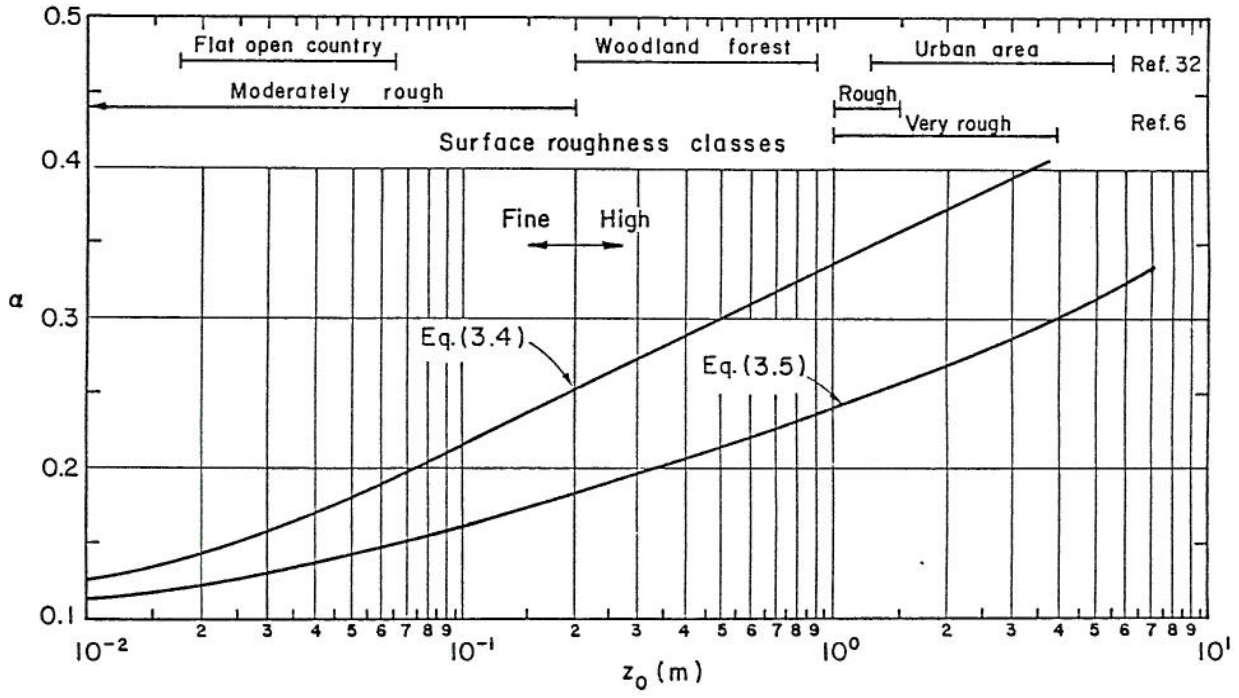

Figure 3.3.3 Variation of the power-law index with increasing roughness and corresponding roughness classes for Equations 3.3.8 and 3.3.9. (Baron, 1981)

Empirical expressions which relate power law index and surface roughness length have been proposed by Counihan (1975) and Baron (1982). Counihan's expression was developed by fitting logarithmic and modified logarithmic profiles to 70 different sites over data to a height of 100 m:

$$\alpha = 0.096 \log_{10} [z_o] + 0.016 (\log_{10} [z_o])^2 + 0.24, \qquad [3.3.8]$$

for $0.001 \leq z_o \leq 5$. Baron fit a similar relationship to the nomogram proposed by Davenport (1975) such that:

$$\alpha = 0.125 \log_{10} [z_o] + 0.0004/z_o + 0.336, \qquad [3.3.9]$$

for a roughness range $0.01 \leq z_o(m) \leq 5.5$. However, the two functions produce significantly different estimates. For example Baron's expression produces power index values 17 to 38% greater than Counihan's expression over the range from smooth to rough roughness **(See Figure 3.3.3)** . This variation may simply be the result of using different data sets, the influence of stratification, or it may be that displacement height was not considered in a similar manner for the two data sets.

Baron (1982) examined a wide cross-section of field and laboratory data and created **Figures 3.3.4 and 3.3.5** which predict power law index in terms of element, h, and roughness height, z_o , respectively. Given canopy heights, h, ranging from 10 to 30 m in depth, associated roughness length, z_o , varying from 1.25 to 3.75 m in size, one expects power law index, α, to vary from 0.45 to 0.52.

3.4 Wind Flow Near Clearings, Clearcuts, and Forest Edges

When airflow passes from a cleared area into a forest winds initially penetrate into the canopy space, but then the streamlines are lifted upward to the canopy roof **(See Figures 3.2.1 and 3.2.2)**. The penetration distance among the trunk space in the canopy understory may persist for 5 to 10 tree heights. Subsequently the wind rises above a recirculation region and re-enters the forest about 20h from the windward forest edge. Cionco (1982) sketched how such entrance flows might look from the perspective of smoke plumes on the battle field in **Figures 3.4.1 and 3.4.2.** But when the airflow passes from a forest canopy to a cleared area the under canopy flow begins to accelerate as much as 5 tree heights upwind as streamlines move toward the ground, but downwind of the forest edge low-level winds may require substantial distance to readjust to the new smaller surface roughness. **(See Figures 3.4.3a and 3.4.3b). Figure 3.4.4** from Meroney (1968) displays the effect of initial wind penetration at the windward forest edge, the low speed recirculating zone, and the flow acceleration before the downstream forest edge on canopy drag. Models which predict wind speed profile variations after changes in roughness are discussed in Section 3.5.

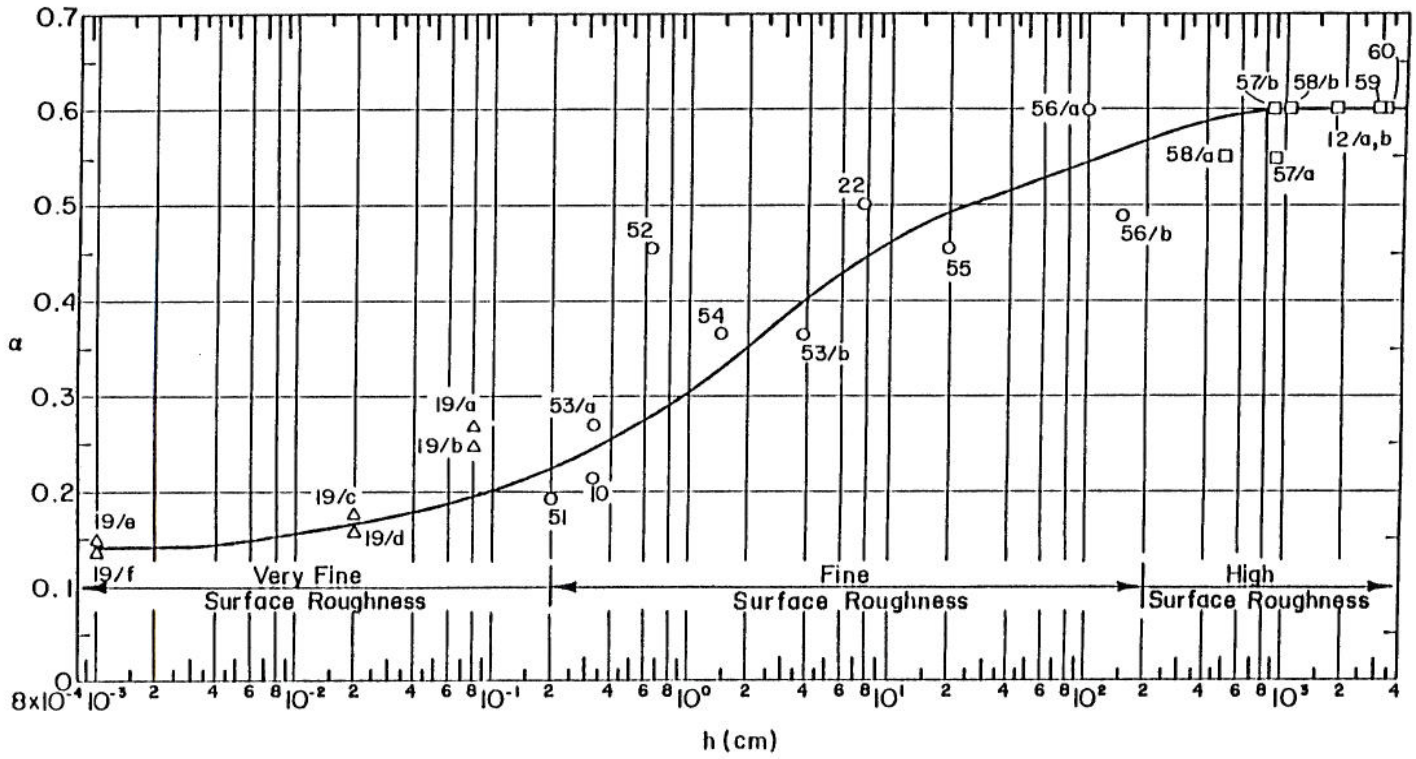

Figure 3.3.4 Variation of the power-law index with increasing height of roughness elements. (Baron, 1981)

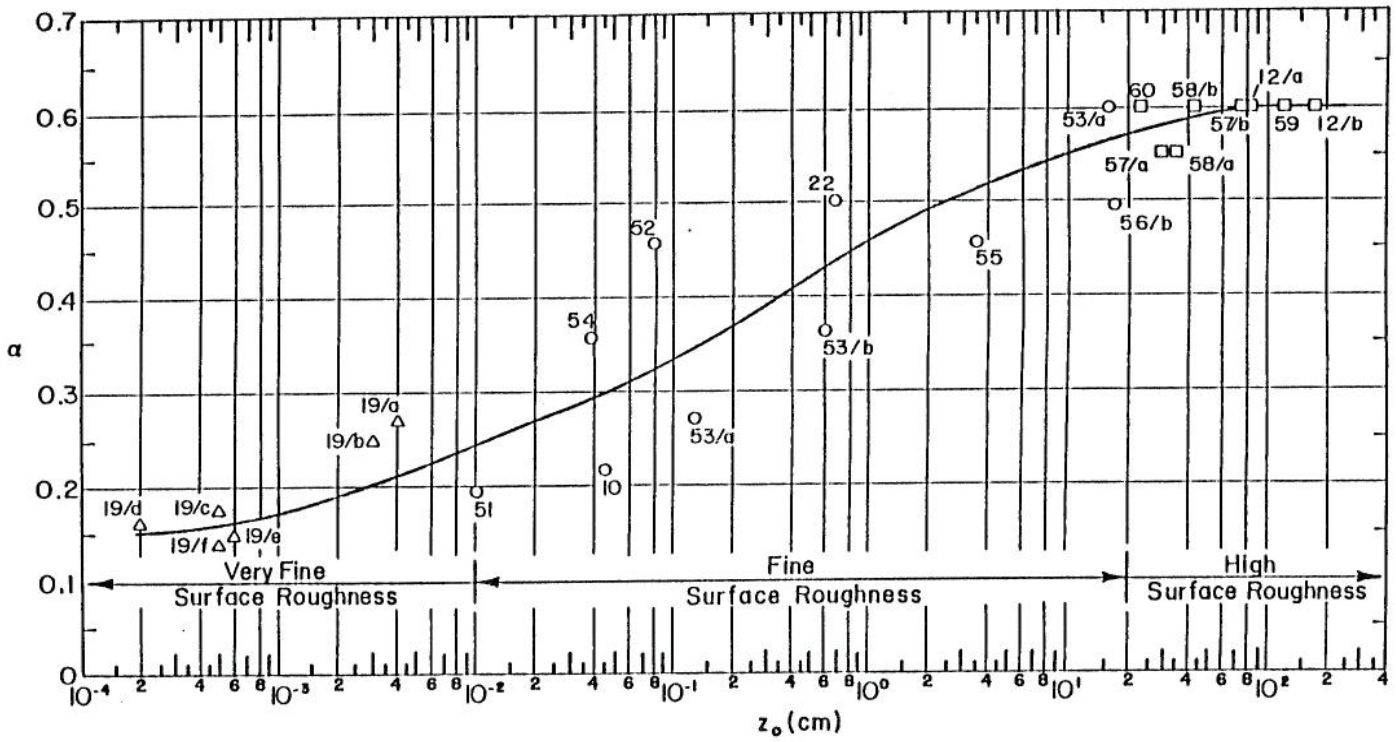

Figure 3.3.5 Variation of the power-law index with increasing roughness length. (Baron, 1981)